JOURNAL OF OPTOELECTRONICS AND ADVANCED MATERIALS Vol. 9, No. 8, August 2007, p. 2555 - 2559

Sol-gel synthesis and characterization of rare-earth doped pure and Gd-substituted YAG

JUNJIE WU, BING YAN*
Department of Chemistry, Tongji University, Shanghai 200092, China

YAG: RE^{3+} (RE= Ce, Tb) and $Y_{3-x}Gd_xAl_5O_{12}$: Tb^{3+} was synthesized by a hybrid precursor assembly sol-gel technology. We get hydroxide sol solutions by stoichiometric aluminum, yttrium, terbium and cerium nitrates, at the same time investigated the relationship between the sol formed and experiment variable including PH, temperature, concentration, and so on. The particle size of luminescent materials is about 100 nm characterized by XRD and especially SEM shows .The co-doping Gd^{3+} and Y^{3+} can't change the crystalline structure in $Y_{3-X}Gd_xAl_5O_{12}$: Tb^{3+}, it also formed the pure-phase YAG. The photoluminescence property of YAG: Tb^{3+} and $Y_{3-x}Gd_xAl_5O_{12}$: Tb^{3+} was compared to investigate as a function of Tb^{3+} ions concentration, which revealed that these phosphors showed the quenching emission for high concentration sample. YAG: Ce^{3+}showed broad emission peaks in the range 480-620 nm and its photoluminescence intensity change alternately with continuous increase in the concentration of Ce^{3+}.

(Received November 16, 2006; accepted June 27, 2007)

Keywords: Sol-gel synthesis, Photoluminescence, Hybrid precursors, Phosphors, Rare earth aluminate

1. Introduction

Luminescent materials which have made greatly progress during the past decades [1, 2] benefit from the improvements in the host materials, so much efforts have been made to discover host materials as well as activator with high performance for phosphor application. All kinds of luminescent materials have their different demand in practice, for example, the cathode ray tube phosphors have been optimized to endure the bombardment of high-voltage electron beams, while field emission display (FED) and plasma displays (PDP) only can work at lower beam energy (3-10 eV) than that required for CRT (20-30 keV) [3-9]. Therefore, there has been an urgent need for the investigation of host materials to meet practical demands. Yttrium aluminum garnet ($Y_3Al_5O_{12}$, YAG) materials have been widely studied in the application of fluorescent and solid state lasers [10-18] because it is a hard material which does not damage easily under conditions of high irradiance with an electron beam. YAG with nice particles size, stable physical and chemical properties leads to being used as a host material for solid lasers, fast flying-spot scanner phosphors and contrast-enhanced display applications. On the other hand, particle sizes affect the photoluminescence intensity of materials. The size of commercial YAG particles is often on the order of 5–20 mm as produced by conventional solid-state reactions at the high temperatures (>1500 °C), which damage the property of products. Finer YAG particles can be synthesized by co-precipitate [19, 20], combustion [21], spray pyrolysis [22] and other methods. YAG as host materials can exhibit full color phosphors by changing the doping rare earth ions such as Eu, Ce, Tb, Sm which broad its application in the field of luminescent materials. It is well known that much more attention has been directed to the sol-gel approach in luminescent materials [23-25] because the direct advantages of this technology include obtaining novel chemical compositions with unique properties, excellent purity and more convenient preparation routes. Through a sol-gel process, it is possible to synthesize phosphors with small size. It is easy to control the composition and homogeneity [26,27]. The active precursors result in low calcination temperature and minimize the potential for cross contamination. Many researchers have done work to synthesize phosphors by sol-gel processing.

In this paper, yttrium, cerium, terbium and gadolinium salicylate coordination polymers were selected as the precursor of luminescent species, polyacrylamide (PAM) as dispersing medium template, $Al(NO_3)_3$ for the sources of the aluminum , and urea for a fuel. These precursors were in situ composed and the luminescent materials YAG: RE^{3+} (RE = Ce, Tb) and Gd-substituted YAG: Tb was achieved by the further thermolysis of the hybrid precursors at 1000 °C, respectively (YAG = $Y_3Al_5O_{12}$). The luminescent performance, structure and grain sizes were systematically examined.

2. Experiment

2.1. Chemicals and procedures

The starting materials Y_2O_3, Ce_2O_4, Gd_2O_3 and Tb_4O_7 were dissolved in diluted HNO_3. The synthesis of

Gd-substituted YAG: Tb^{3+} and YAG: RE^{3+} (RE = Ce, Tb) by rare earth salicylate coordination polymer-PAM precursors were described in the following: excess salicylic acid (5.0 mmol) was dissolved into 95 % ethanol and its pH value 10 ml solution was adjusted to be about 7.0 with ammonia solution. Then mixed solutions of rare earth nitrates (with the molar ratio of Ce:Y = 0.02, 0.03, 0.05, 0.07, 0.09) were added and mixed homogenously. The solutions of urea, PAM and $Al(NO_3)_3$ were added into the above solution. Heating and stirring for about 4 hrs at 80 °C, light yellow gel were obtained, dried and the precursors were achieved. The hybrid precursors were calcinated in a resistance stove for 4 hrs at 1000 °C. The typical synthesis procedure can be shown in the following: (taking Gd-substituted YAG: Tb^{3+} for example)

$$xY(NO_3)_3 + (3\text{-}x)Gd(NO_3)_3 + (0.01\text{-}0.07)Tb(NO_3)_3 + 9.6HSal + NH_3{\bullet}H2O$$

$$\rightarrow [Y_{3-x}Gd_xTb(Sal)_3]_n + 5Al(NO_3)_3 + 5.0\ PAM + 5.0\ NH_2\text{-}CO\text{-}NH_2 + NH_3{\bullet}H_2O$$

$$\rightarrow Y_{3-x}Gd_xTbAl_5O_{12} + CO_2\uparrow + NH_3\uparrow + NO_2\uparrow + H_2O\uparrow$$

2.2. Physical measurements

The particle size was characterized by means of X-ray diffraction (XRD, Bruke, D8-Advance, 40 Kv and 20 mA, Cukα). The morphology and microstructure were characterized with scanning electronic microscope (SEM, Philips XL-30). Excitation and emission spectra at room temperature were determined with Perkin-Elmer LS-55 model fluorophotometer (scan rate = 1500 nm/s, excitation slit width = 10 nm, emission width = 5 nm).

3. Results and discussion

The XRD patterns for these phosphors were measured and exhibited similar crystalline structure. Fig.1 presents the selected XRD patterns of the YAG: Ce^{3+} (A), YAG: Tb^{3+} (B) and $Y_{3-x}Gd_xAl_5O_{12}$:Tb^{3+} (C) crystalline powders calcined at 1000 °C for 4 hours, respectively. The diffraction patterns for YAG: RE^{3+} (RE = Ce, Tb) and $Y_{3-x}Gd_xAl_5O_{12}$: Tb^{3+} was found to be exactly the same as that of $Y_3Al_5O_{12}$ reported in JCPDS Card. It is well known that Y^{3+} and Gd^{3+} have similar character, so the crystal structure will remain constant when Gd^{3+} ions substituted for Y^{3+} ions. Co-doping Gd^{3+} concentration is low, Gd^{3+} replaced the sites of Y^{3+} in the crystal structure, so the phases maintain as that of YAG. When the concentration of Gd^{3+} is large, there are some other crystal phases such as Gd_2O_3, Al_2O_3 as it shows in Fig. 1(C). The reason, we believe lies in as following: Gd^{3+} takes up the site of Al^{3+} in the crystal lattice, so AlO_4^- break down and Gd_2O_3, Al_2O_3 come into being. The crystal size was estimated from the broadening of the peaks by using the Scherrer formula:

$$D_{hkl} = k\lambda / [\alpha(2\theta)\cos\theta] \quad (1)$$

where β (2θ) is the width of the pure diffraction profile in radians, k is 0.89, λ is the wavelength of the X-rays (0.154056 nm), θ is the diffraction angle, and D_{hkl} is the age diameter of the crystallite. By fitting various peaks to this formula and taking into account the instrumental broadening, it can be found that the particles is about 100 nm. According to some other researchers reported, the phase-pure particles were formed after annealing at 1000 °C, because of good mixing of each component on the scale of several nanometers. The reason, we believe that by using sol-gel phosphors, materials can be formed at lower temperature than those of conventional solid-state reaction method above 1500 °C.

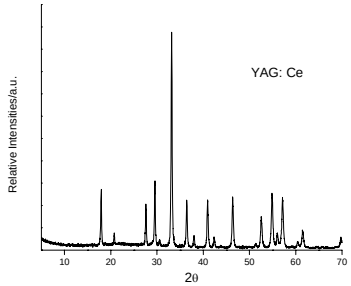

(a)

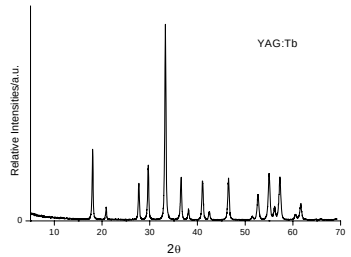

(b)

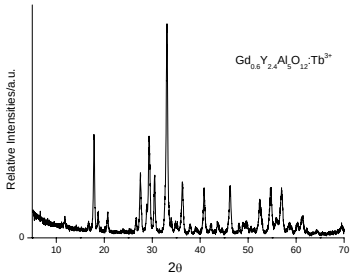

(c)

Fig. 1. The XRD patterns of the YAG: Ce^{3+} (A), YAG: Tb^{3+} (B) and $Y_{3-x}Gd_xTbAl_5O_{12}$: Tb^{3+} (C) crystalline powders.

We further used the scanning electron microscope (SEM) to measure the YAG: Ce^{3+}, YAG: Tb^{3+} and $Y_{3-x}Gd_xTbAl_5O_{12}$: Tb^{3+} samples. Fig. 2 show the representative SEM micrograph for YAG: Ce^{3+} (A), YAG: Tb^{3+} and $Y_{3-x}Gd_xTbAl_5O_{12}$: Tb^{3+} (B), respectively. It can be seen that all products mainly consist of solid micron crystalline structures, which exhibit an interpenetrating network structures for the high temperature 1000 ℃ of thermal decomposition. The typical particle is estimated to be about 100 nm in dimension. Besides this, the three-dimensional sizes of crystalline are very thick to afford high strength it need to refer these powders with high strength would be very useful for the application to obtain high efficient phosphors because these microcrystalline materials can result in high luminescent intensities [28].

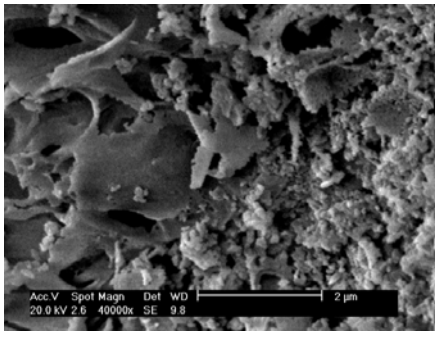

(a)

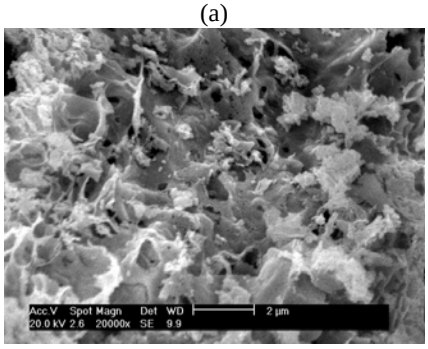

(b)

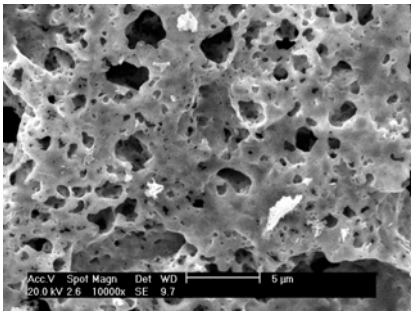

(c)

Fig. 2. SEM of YAG: Ce^{3+} (A), YAG: Tb^{3+} (B), and (C) and $Y_{3-x}Gd_xTbAl_5O_{12}$: Tb^{3+} (C).

Fig. 3 shows the excitation spectra of YAG: Ce^{3+} (A) YAG: Tb^{3+} (B), that of $Y_{3-x}Gd_xTbAl_5O_{12}$: Tb^{3+} is similar to that of YAG: Tb^{3+}. The excitation spectra of YAG: Ce^{3+} consists of three broad bands with maxima at 286, 343 and 456 nm between 200 and 500 nm as it shown in Fig. 3 (A). We can understand this phenomenon from the electronic structure of Ce^{3+}. Trivalent Cerium only has one electron in the 4f state. The ground state of Ce^{3+} is split into $^2F_{7/2}$ and $^2F_{5/2}$ with and energy difference of about 2200 cm^{-1} [29]. The higher state originates from the 5d state and 4f-5d transitions are allowed. The 5d state is splited by crystal field and there is more than one absorption band in the region from 200 nm to 500 nm. The representative excitation spectrum for YAG: Tb^{3+} and $Y_{3-x}Gd_xTbAl_5O_{12}$: Tb^{3+} is shown in Fig. 3 (B), which is taken at an emission wavelength of 545 nm. There exist some broad bands (269, 303, 357.5, 412.5, 454, 480 nm) between 200 and 500 nm. The weak bands centered at 269 nm owe to the 9D level of the 4f7-5d1 configurations by the considering spin selection rule, which the oscillator originated from a spin-forbidden transition. The broad band situated the region between 300 and 500 nm comes from the 4f-4f transitions within the Tb^{3+} electron configuration in long wavelength range.

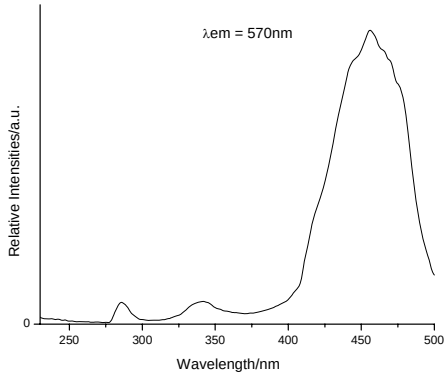

(a)

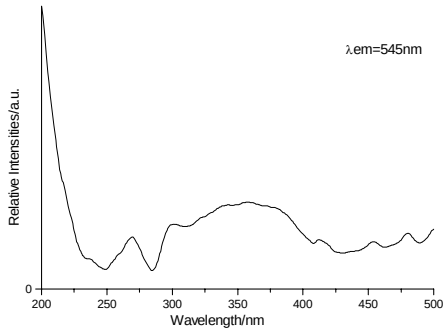

(b)

Fig. 3. Excitation spectra of YAG: Ce^{3+} (A) and YAG: Tb^{3+}, $Y_{3-x}Gd_xTbAl_5O_{12}$: Tb^{3+} (B).

The luminescence properties of Ce^{3+} are different when we change the doping concentration in the host lattices. Fig. 4 shows the emission spectra of YAG: Ce^{3+} (0.02, 0.03, 0.05, 0.07, 0.09). When the concentration of Ce^{3+} increases up to 0.03 (3 mol %), the corresponding phosphor exhibits the strongest emission and the emission intensity decreases alternately with continuous increase in the concentration of Ce^{3+}. At the concentration of Ce^{3+} reaches 5 mol %, the phosphor shows weaker emission intensity, and so the concentration quenching effect takes place. Moreover, the doping concentration has only little influence on the corresponding intensities and the distinction of luminescence intensities for different doping concentrations.

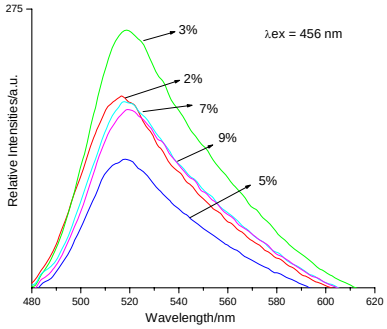

Fig. 4. Emission spectrum of YAG: xCe^{3+} (x = 0.02, 0.03, 0.05, 0.07, 0.09 mmol).

Fig. 5 shows the emission spectra of YAG: Tb^{3+} (0.01, 0.02, 0.03, 0.05). It can be found that the emission spectra consist of four peaks situated at 485, 542.5, 594, 620 nm which agree with the mechanism of Tb3+ activator. As we known, the emission lines of Tb in these compounds originate mainly from the transitions of $^5D_3$–^7F_J (J = 6, 5, 4, 3) and $^5D_4$–^7F_J [11]. It can be seen that the fluorescence spectra of the as-prepared phosphors are dominated by the $^5D_4$ emission. The dominant peak is located 594 nm attributed to electron transition $^5D_4$-$^7F_4$. The emission intensity increase with improving the Tb^{3+} while the strong emission appears by doping with 5 mol % Tb^{3+}.

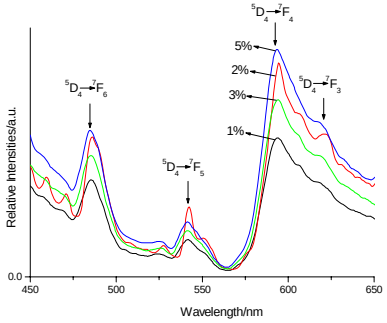

Fig. 5. Emission spectrum of YAG: Tb^{3+} (x = 0.01, 0.02, 0.03, 0.05 mmol).

Fig. 6 compared the luminescent intensities with different composition of host matrix in $Y_{3-x}Gd_xTbAl_5O_{12}$ (doping the same ratio of Tb^{3+} (2 mol %)). The emission spectra are composed of $^5D_4$-^7F_J (J = 6, 5, 4, 3) emission lines of Tb^{3+}, with the hypersensitive emission transition $^5D_4$-$^7F_6$ being the most prominent group, whose peaks situated at 485 nm. There is some different from that in YAG: Tb^{3+}, the reason, we believe lies in that the radius of Gd^{3+} is larger than Y^{3+} in an octahedral coordinated site. As a result, the unit cell becomes larger, and the lowest sublevel of the 5d state of Tb^{3+} becomes further lower in energy due to a stronger crystal field when Gd^{3+} substitutes Y^{3+}. On the other hand, we investigate the spectra of Ce^{3+} and Gd^{3+} co-doping in YAG (not shown). It can be seen that the spectra is different from that not only in YAG: Tb^{3+} but also in YAG: Ce^{3+}. Its shape and situation have some change. The reason lies in the factors as following: the transfer of energy from the Ce^{3+} to Tb^{3+} lattice ion due to a slight overlap of the Ce^{3+} luminescence in YAG: Tb^{3+} with the ^7F_J-$^5D_4$ absorption band of Tb^{3+}. When the ratio of Tb^{3+} and Ce^{3+} is 5 to 2, the products exhibit the strongest emission.

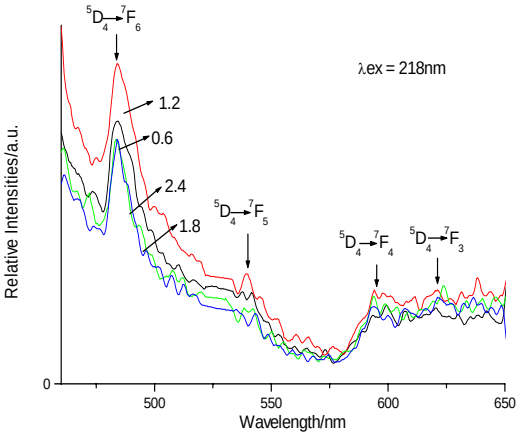

Fig. 6. Luminescence intensities of $Y_{3-x}Gd_xTbAl_5O_{12}$: Tb^{3+} (x = 0.6, 1.2, 1.8, 2.4).

4. Conclusion

In summary, YAG: RE^{3+} (RE = Ce, Tb) and Gd-substituted YAG: Tb^{3+} was synthesized by composing hybrid precursors at 1000 ºC for 4 hours, both XRD and SEM results indicate that these phosphors exhibit interpenetrating network structures with micrometer dimension. YAG: RE^{3+} (RE = Ce, Tb) and $Y_{3-x}Gd_xTbAl_5O_{12}$: Tb^{3+} appear the concentration quenching phenomenon at the range of 1.0-10 mol % of activator ions and co-doping Ce^{3+} and Gd^{3+} can change the emission spectra.

Acknowledgements

The work was supported by the Science of Shanghai University for Excellent Youth Scientists and National Natural Science Foundation of China (20671072).

References

[1] D. M. Burland, R. D. Miller, C. A. Walsh, Chem. Rev. **94**, 31 (1994).
[2] L. L. Beecroft, C. K. Ober, Chem. Mater. **9**, 1302 (1997).
[3] X. M. Liu, Y. Luo, J. Lin, J. Cryst. Growth. **290**, 266-271 (2006).
[4] A. Nag, T. R. N. Kutty, J. Phys. Chem. Solids. **191-199**, 66 (2005).
[5] D. S Xing, K. W. Cheah, P. Y Cheng, J Xu, Solid. State. Commun. **134**, 809-813 (2005).
[6] M. G. Ko, J. C. Park, D. K. Kim, S. H. Byeon, J. Lumin. **104**, 215-221 (2003).
[7] F. Zhao, P. M. Guo, G. B. Li, F. H. Liao, S. J Tian, X. P. Jing, Mater. Res. Bull. **38**, 931-940 (2003).
[8] J. Mckittrick, L. E. Shea, C. F. Bacalski, E. J. Bosze, Display. **19**, 169-172 (1999).
[9] O. A. Lopez, J. McKittrick, L. E. Shea, J. Lumin. **71**, 1 (1997).
[10] X. Li, Q. Li, J. Y. Wang, S. L. Yang, Mater. Sci. Eng. B. **131**, 32-35 (2006).
[11] X. Li, H. Liu, J. Y. Wang, H. M. Cui, S. L. Yang, I. R. Boughton, J. Phys. Chem. Solids. **66**, 201-205 (2005).
[12] J. J. Zhang, J. W. Ning, X. J. Liu, Y. P. Pan, L. P. Huang, Mater. Res. Bull. **38**, 1249-1256 (2003).
[13] Y. Hakuta, T. Haganuma, K. Sue, T. Adschiri, K. Arai, Mater. Res. Bull. **38**, 1257-1265 (2003).
[14] J. Y. Choe, D. Ravichandran, S. M. Blomquist, K. W. Kirchner, E. W. Forsythe, D. C. Morton, J. Lumin. **93**, 119-128 (2001).
[15] Y. Zorenko, V. Gorbenko, I. Konstankevych, A. Voloshinovskii, G. Stryganyuk, V. Mikhailin, V. Kolobanov, D. Spassky, J. Lumin. **114**, 85-89 (2005).
[16] G. Del Rosario, S. Ohara, L. Mancic, O. Milosevic, Appl. Surf. Sci. **238**, 469-474 (2004).
[17] M. Batentschuk, A. Osvet, G. Schierning, A. Klier, J. Schneider, A. Winnacker, Radiat. Meas. **38**, 539-543 (2004).
[18] D. Ravichandran, R. Roy, A.G. Chakhovskoi, C. E. Hunt, W. B. White, S. Erdei, J. Lumin. **71**, 291 (1997).
[19] T. M. Chen, S. C. Chen, C. J. Yu, J. Solid State Chem. 144, 437–441 (1999).
[20] H. Wang, L. Gao, K. Niihara, Mater. Sci. Eng. A **288**, 1-4 (2000).
[21] S. Shi, J. Wang, J. Alloys Comp. **327**, 82-86 (2001).
[22] Y. C. Kang, I. W. Lenggoro, S. B. Park, K. Okuyama, Mater. Res. Bull. **35**, 789-798 (2000).
[23] L. R. Matthews, E. T. Knobbe, Chem. Mater. **5**, 1697 (1993).
[24] U. A. Serra, E. J. Nassar, G. Zapparolli, J. Alloys Compd. **207/208**, 454 (1994).
[25] R. Campostrini, G. Carturn, M. Ferrari, M. Motagna, O. Pilla, J. Mater. Res. 1992; 7.
[26] H. H. Huang, B. Yan, J. Mater. Sci. Lett. **39**, 3529 (2004).
[27] H. H. Huang, B. Yan, Inorg. Chem. Commun. **7**, 919 (2004).
[28] P. S. Pizani, E. R. Leite, F. M. Pontes, E. C. Paris, J. H. Rangel, J.H. Lee, E. Longo, P. Delega, J. A. Varela, Appl. Phys. Lett. **77**, 824 (2000).
[29] Y. X. Pan, M. M. Wu, Q. Su, J. Phys. Chem. Solids. **65**, 845-850 (2004).

*Corresponding author: byan@tongji.edu.cn